Reconsideration of X, the Diiron Intermediate Formed during Cofactor Assembly in *E. coli* Ribonucleotide Reductase

Bradley E. Sturgeon,[†] Doug Burdi,[‡] Shuxian Chen,[§] Boi-Hanh Huynh,*[,§] Dale E. Edmondson,[⊥] JoAnne Stubbe,*[,‡] and Brian M. Hoffman*[,†]

Contribution from the Department of Chemistry, Northwestern University, Evanston, Illinois 60208-3113, Department of Chemistry, Massachusetts Institute of Technology, Cambridge, Massachusetts 02139, and Departments of Physics and Biochemistry, Emory University, Atlanta, Georgia 30322

Received February 7, 1996[⊗]

Abstract: The R2 subunit of *Escherichia coli* ribonucleotide reductase (RNR) contains a stable tyrosyl radical (•Y122) diferric cluster cofactor. Earlier studies on the cofactor assembly reaction detected a paramagnetic intermediate, **X**, that was found to be kinetically competent to oxidize Y122. Studies using rapid freeze-quench (RFQ) Mössbauer and EPR spectroscopies led to the proposal that **X** is comprised of two high spin ferric ions and a $S = 1/2$ ligand radical, mutually spin coupled to give a $S = 1/2$ ground state (Ravi, N.; Bollinger, J. M., Jr.; Huynh, B. H.; Edmondson, D. E.; Stubbe, J. *J. Am. Chem. Soc.* **1994**, *116*, 8007−8014). An extension of RFQ methodology to Q-band ENDOR spectroscopy using ^{57}Fe has shown that one of the irons has a very nearly isotropic hyperfine tensor ($\mathbf{A}(Fe_A) = -[74.2(2), 72.2(2), 73.2(2)]$ MHz) as expected for Fe^{III}, but that the other iron site displays considerable anisotropy ($\mathbf{A}(Fe_B) = +[27.5(2), 36.8(2), 36.8(2)]$ MHz), indicative of substantial Fe^{IV} character. Reanalysis of the Mössbauer data using these results leads to isomer shifts of $\delta(Fe_A) = 0.56(3)$ mm/s and $\delta(Fe_B) = 0.26(4)$ mm/s. Based on the hyperfine anisotropy of Fe_B plus the reduced isomer shift, **X** is now best described as a spin-coupled Fe^{III}/Fe^{IV} center without a radical, but with significant spin delocalization onto the oxygen ligand(s).

Ribonucleotide reductases (RNR) catalyze the conversion of nucleotides to 2′-deoxynucleotides in a process that constitutes the rate-limiting step of DNA biosynthesis.[1−4] The RNR from *E. coli* contains two homodimeric subunits. The larger subunit, R1, contains the active site, binding sites for the allosteric effectors, and the five cysteine residues[5−8] that are required for catalysis. The R2 subunit contains a catalytically essential, stable tyrosyl radical located on residue 122 (•Y122)[9] adjacent (5.3 Å) to a μ-oxo, carboxylato-bridged diferric cluster.[10] The crystallographic determination of the structures of R1 and R2[10,11] has allowed docking of the two subunits and indicates a distance between the cofactor of R2 and the active site in R1 of ∼35 Å! These observations along with extensive biochemical evidence have led us[7,12] and others[10] to propose that •Y122 functions as the "pilot light" that initiates catalysis via a long-range, proton-coupled electron transfer between subunits, to form a thiyl radical[12] on C439 of R1 that ultimately initiates the nucleotide reduction process.

Although the diiron cluster of RNR plays no *recurring* role in the enzyme's catalytic cycle, much interest in its biosynthesis has been evoked by its unusual structure and requirement for generation of the essential tyrosyl radical. Seminal experiments of Atkin et al.[13] demonstrated that incubation of apo-R2 with Fe^{2+}, O_2, and reductant results in cofactor formation. The stoichiometry of this reconstitution reaction has been examined[14−17] and is indicated in eq 1.

$$\text{apo R2-Y122} + 2Fe^{2+} + 1H^+ + O_2 + 1e^- \rightarrow R2(Fe^{3+})_2O/Y122^\bullet + H_2O \quad (1)$$

These studies revealed the requirement of one electron, in addition to those provided by $2Fe^{2+}$ and Y122, to complete the net four-electron reduction of dioxygen to water and create the tyrosyl radical and diferric cluster. The reason why the diferrous center in R2 shows this unique chemical reactivity, in contrast to the reversible O_2 binding by the diferrous center of hemerythrin[18−20] and the hydroxylation of unactivated carbon−hydrogen bonds by the corresponding center of methane

[†] Northwestern University.
[‡] Massachusetts Institute of Technology.
[§] Department of Physics, Emory University.
[⊥] Department of Biochemistry, Emory University.
[⊗] Abstract published in *Advance ACS Abstracts,* July 15, 1996.

(1) Fontecave, M.; Nordlund, P.; Eklund, H.; Reichard, P. *Adv. Enzymol. Relat. Areas Mol. Biol.* **1992**, *65*, 147−183.
(2) Eriksson, S.; Sjöberg, B. M. In *Allosteric Enzymes*; Hervé, G., Ed.; CRC Press: Boca Raton, FL, 1989; pp 189−215.
(3) Stubbe, J. *Adv. Enzymol. Relat. Areas Mol. Biol.* **1990**, *63*, 349−419.
(4) Reichard, P. *Science* **1993**, *260*, 1773−1777.
(5) Mao, S. S.; Holler, T. P.; Yu, G.-X.; Bollinger, J. M., Jr.; Booker, S.; Johnston, M. I.; Stubbe, J. *Biochemistry* **1992**, *31*, 9733−9743.
(6) Mao, S. S.; Holler, T. P.; Bollinger, J. M., Jr.; Yu, G.-X.; Johnston, M. I.; Stubbe, J. *Biochemistry* **1992**, *31*, 9744−9751.
(7) Mao, S. S.; Yu, G.-X.; Chalfoun, D.; Stubbe, J. *Biochemistry* **1992**, *31*, 9752−9759.
(8) Åberg, A.; Hahne, S.; Karlsson, M.; Larsson, Å.; Ormö, M.; Åhgren, A.; Sjöberg, B.-M. *J. Biol. Chem.* **1989**, *264*, 12249−12252.
(9) Larrson, Å.; Sjöberg, B. M. *EMBO J.* **1986**, *5*, 2037−2040.
(10) Nordlund, P.; Eklund, H. *J. Mol. Biol.* **1993**, *232*, 123−164.
(11) Uhlin, U.; Eklund, H. *Nature* **1994**, *370*, 533−539.
(12) Stubbe, J. *J. Biol. Chem.* **1990**, *265*, 5329−5332.
(13) Atkin, C. L.; Thelander, L.; Reichard, P.; Lang, G. *J. Biol. Chem.* **1973**, *248*, 7464−7472.
(14) Bollinger, J. M., Jr.; Edmondson, D. E.; Huynh, B. H.; Filley, J.; Norton, J. R.; Stubbe, J. *Science* **1991**, *253*, 292−298.
(15) Lynch, J. B.; Juarez-Garcia, C.; Münck, E.; Que, L., Jr. *J. Biol. Chem.* **1989**, *264*, 8091−8096.
(16) Bollinger, J. M., Jr. Ph.D. Thesis, Massachusetts Institute of Technology, 1993.
(17) Bollinger, J. M., Jr.; Tong, W. H.; Ravi, N.; Huynh, B. H.; Edmondson, D. E.; Stubbe, J. *J. Am. Chem. Soc.* **1994**, *116*, 8015−8023.
(18) Shiemke, A. K.; Loehr, T. M.; Sanders-Loehr, J. *J. Am. Chem. Soc.* **1984**, *106*, 4951−4956.
(19) Stenkamp, R. E.; Sieker, L. C.; Jensen, L. H.; McCallum, J. D.; Sanders-Loehr, J. *Proc. Natl. Acad. Sci. U.S.A.* **1985**, *82*, 713−716.
(20) Shiemke, A. K.; Loehr, T. M.; Sanders-Loehr, J. *J. Am. Chem. Soc.* **1986**, *108*, 2437−2443.

S0002-7863(96)00399-X CCC: $12.00

Scheme 1

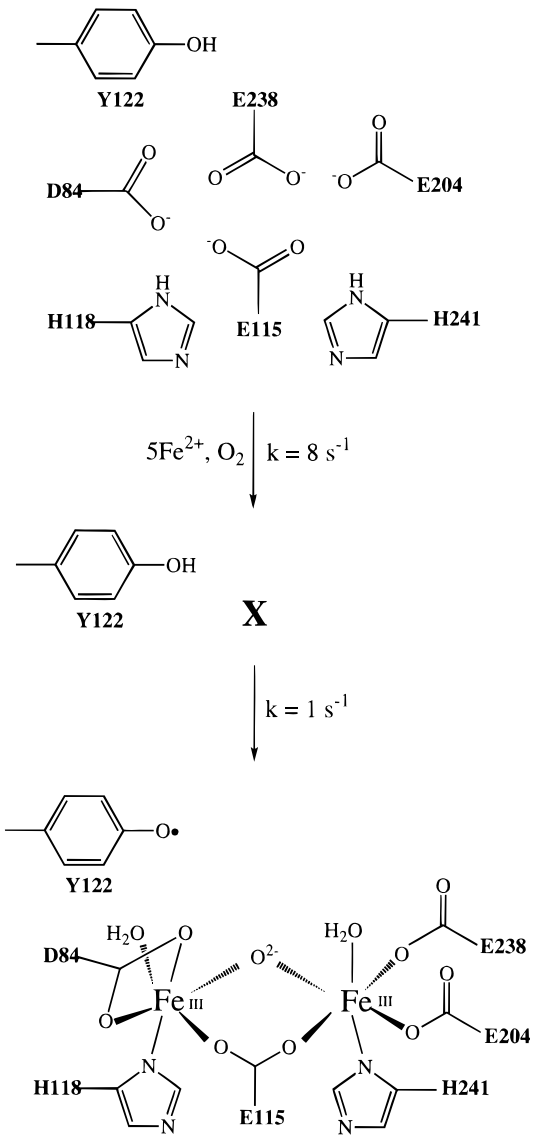

monooxygenase,[21−24] remains enigmatic, despite having been studied by many investigators.[25,26]

The ability to reconstitute R2 of RNR with Fe^{2+} and O_2 plus the experimental determination of the stoichiometry in eq 1 provided the foundation for a mechanistic investigation of the self-assembly reaction. In 1991, Bollinger et al.[14] examined this process by stopped-flow (SF) UV−vis spectroscopy and rapid freeze-quench (RFQ) EPR and Mössbauer spectroscopies.[27] In the presence of excess reductant, a paramagnetic intermediate (**X**) was detected that is kinetically competent to oxidize Y122. A kinetic analysis[17] revealed that **X** is generated with a rate constant of 8 s^{-1} and decomposes with a rate constant of 1 s^{-1}, the same rate constant associated with tyrosyl radical formation (Scheme 1). To facilitate the characterization of **X** by spectroscopic methods, site-specific mutagenesis was used to replace Y122 with the less easily oxidized phenylalanine,[14,28] allowing the generation of stoichiometric amounts (1.02 equiv/R2)[29,30] of intermediate.

The studies of **X** using the spectroscopic methods enumerated above have shown that it has a UV−vis absorption feature at 365 nm and a narrow, free-radical-like X-band EPR signal that ^{57}Fe-labeling experiments reveal is associated with an iron cluster. The intermediate is formally at a Fe^{III}/Fe^{IV} level of oxidation, that is, oxidized by 1 equiv relative to the diferric cluster in the resting state of R2. Mössbauer measurements and analysis assuming isotropic magnetic hyperfine coupling tensors for both iron sites established that **X** contains two antiferromagnetically exchange-coupled Fe ions, with isomer shifts that were found to be 0.55 and 0.36 mm s^{-1}. These studies led to a proposal[31,32] that **X** is comprised of two high spin ferric ions and a $S = 1/2$ ligand radical, mutually spin coupled to give a $S = 1/2$ ground state. The formulation of **X** as a diferric radical stood in contrast to the high valent iron-oxo species postulated by many investigators[33−35] based on analogies with heme systems.

Recently, further characterization of **X** has been undertaken using RFQ ENDOR spectroscopy.[36] Studies using $^{17}O_2$ and $H_2{}^{17}O$ have revealed that at least one atom of oxygen from O_2 and one from H_2O are present in **X**. We have extended these studies to RFQ ^{57}Fe ENDOR in order to accurately measure the iron hyperfine couplings, assumed to be isotropic in the original formulation of **X** as a diferric radical. The ^{57}Fe ENDOR measurements disclose that the hyperfine tensor of one of the Fe ions is markedly anisotropic, indicative of substantial Fe^{IV} character. Using the ENDOR results, we have reanalyzed the Mössbauer data. The results of both the ENDOR experiments and Mössbauer analysis now indicate that this intermediate is best described as a spin-coupled Fe^{III}/Fe^{IV} diiron center without a radical but with significant spin delocalization onto the oxygen ligand(s).

Materials and Methods

Materials. ^{57}Fe was purchased from Advanced Materials and Technology (New York, NY). 2-Methylbutane (reagent grade) was purchased from Aldrich (Milwaukee, WI).

Preparation of ^{57}Fe Stock Solution. A nugget of ^{57}Fe metal (3.3 mg, 57.9 μmol) was suspended in 130 μL of argon-saturated 2 N H_2SO_4 in an Eppendorf tube sealed tightly with a septum. The container was flushed with argon. After 30 min at 60 °C, the solution was removed via gas-tight syringe, and a fresh 130 μL aliquot was added. The reaction was allowed to proceed for 48 h at 60 °C at which point the solution was cooled and centrifuged to pellet any undissolved metal. A 120 μL aliquot of the supernatant was diluted to a volume of 5.0 mL with argon-saturated H_2O. A ferrozine assay[37−39] revealed an Fe^{2+} concentration of 10.5 mM; the concentration of H_2SO_4 was calculated to be 27 mN.

(21) Dalton, H. *Adv. Appl. Microbiol.* **1980**, *26*, 71−87.
(22) Fox, B. G.; Dege, J. E.; Froland, W. A.; Lipscomb, J. D. *J. Biol. Chem.* **1989**, *264*, 10023−10033.
(23) Liu, K. E.; Valentine, A. M.; Wang, D.; Huynh, B. H.; Edmondson, D. E.; Salifoglou, A.; Lippard, S. J. *J. Am. Chem. Soc.* **1995**, *117*, 10174−10185.
(24) Rosenzweig, A. C.; Nordlund, P.; Takahara, P. M.; Frederick, C. A.; Lippard, S. J. *Chem., Biol.* **1995**, *2*, 409−418.
(25) Kurtz, D. M., Jr. *Chem. Rev.* **1990**, *90*, 585−606.
(26) Feig, A. L.; Lippard, S. J. *Chem. Rev.* **1994**, *94*, 759−805.
(27) Bollinger, J. M., Jr.; Tong, W. H.; Ravi, N.; Huynh, B. H.; Edmondson, D. E.; Stubbe, J. In *Methods in Enzymology*; Klinman, J. P., Ed.; Academic Press: New York, 1995; p 258.
(28) Bollinger, J. M., Jr.; Stubbe, J.; Huynh, B. H.; Edmondson, D. E. *J. Am. Chem. Soc.* **1991**, *113*, 6289−6291.
(29) Tong, W. H. Ph.D. Thesis, Massachusetts Institute of Technology; **1996**.
(30) Tong, W. H.; Burdi, D.; Daniel, R.; Lloyd, S.; Edmondson, D. E.; Huynh, B. H.; Stubbe, J. Manuscript in preparation.
(31) Ravi, N.; Bollinger, J. M., Jr.; Huynh, B. H.; Edmondson, D. E.; Stubbe, J. *J. Am. Chem. Soc.* **1994**, *116*, 8007−8014.
(32) Ravi, N.; Bominaar, E. L. *Inorg. Chem.* **1995**, *34*, 1040−1043.
(33) Que, L. *Science* **1991**, *253*, 273.
(34) Ling, J.; Sahlin, M.; Sjöberg, B. M.; Loehr, T. M.; Sanders-Loehr, J. *J. Biol. Chem.* **1994**, *269*, 5595−5601.
(35) Fontecave, M.; Gerez, C.; Atta, M.; Jeunet, A. *Biochem. Biophys. Res. Commun.* **1990**, *168*, 659−664.
(36) Burdi, D.; Sturgeon, B. E.; Tong, W. H.; Stubbe, J.; Hoffman, B. M. *J. Am. Chem. Soc.* **1996**, *118*, 281−282.
(37) Salowe, S. P. Ph.D. Thesis, University of Wisconsin, 1987.
(38) Stookey, L. L. *Anal. Chem.* **1970**, *42*, 779−781.
(39) Massey, V. J. *J. Biol. Chem.* **1957**, *229*, 763−770.

Preparation of Apo Y122F. A site-directed mutant, R2-Y122F, was used in this study in order to remove the paramagnetic signal contributed by the tyrosyl radical in the wild-type R2.[40] R2-Y122F was isolated from the overproducing strain K38/pGP1−2/pTB2(Y122F) as described previously.[17] Apo-Y122F R2 was prepared from its iron-containing precursor using a modified[37] chelation procedure of Atkin.[13] The concentration of apo-R2 was determined by A_{280} (ϵ = 120 mM^{-1} cm^{-1}).[41]

General Procedure for the Preparation of ^{57}Fe RFQ Q-Band ENDOR Samples. The method for preparing RFQ Q-band ENDOR samples is similar to the technique previously described[27,42,43] for the preparation of RFQ EPR samples. The RFQ instrument consists of an Update Instruments Drive Ram assembly, a Model 715 computer controller, and a quenching bath. The bath holds 8 L of isopentane which was cooled to and maintained at −140 °C using liquid nitrogen. A Pyrex funnel was fabricated such that the inner diameter of its fluted end matched that of the ENDOR sample tube. The funnel was then connected via a latex collar to a Q-band ENDOR tube (2.5 mm od/2.0 mm id), and the assembly was filled with isopentane and immersed in the cooling bath where it was allowed to reach thermal equilibrium. One drive syringe of the ram unit was loaded with apo R2-Y122F (600 μM) in oxygen-saturated HEPES (100mM; pH 7.7), and the other was loaded with a solution of $^{57}Fe^{2+}$ (3.00 mM) in oxygen-saturated 8.5 mN H_2SO_4. The apparatus was cooled to 5 °C. The reconstitution reaction was initiated by actuation of the ram drive, and the two reactants were mixed rapidly and efficiently in a mixing chamber. The quench time for the reaction could be precisely controlled by varying both the speed of the drive ram and the length of the aging loop. For these studies, a quench time of 610 ms was selected. After the reaction mixture traversed the aging loop, it was shot out of a nozzle into the sample funnel containing the cold isopentane. The resulting snow-like crystals were packed into the bottom of the ENDOR tube using a stainless steel packer which was fabricated from 1/16" stock. A ram speed of 1 cm s^{-1} produced ice crystals which were suitable for packing. The excess isopentane was then carefully removed, and, while maintaining the sample at liquid nitrogen temperature, the funnel and latex collar were disconnected. Neglecting the volume remaining in the aging loop, a final sample volume of about 170 μL was required to generate each sample.

Q-Band EPR and ENDOR Spectroscopy. Continuous-wave EPR spectra were recorded at 2 K on a modified Varian E109 EPR spectrometer equipped with an E110 35 GHz microwave bridge in the dispersion mode, using 100-kHz field modulation under conditions of rapid passage as described elsewhere.[44] In this detection scheme the signal approximates to the undifferentiated EPR absorption envelope; derivative presentations, when desired, were obtained by numerical differentiation. The ENDOR response was observed as rf-induced changes in the dispersion-EPR intensity. ENDOR signal/noise ratios were enhanced by broadening the radiofrequency with a white noise source (bandwidth ∼ 100 kHz).[45]

In a frozen metalloenzyme solution, all possible orientations of molecules with respect to the applied magnetic field are present and contribute to the EPR spectrum. To determine the full hyperfine tensor of each nucleus, including its orientation with respect to the *g* tensor frame, ENDOR spectra are collected across the whole EPR envelope and analyzed as described elsewhere.[46−48]

Mössbauer Spectroscopy. The Mössbauer sample was prepared from apo R2-Y122F and recorded as described previously.[31]

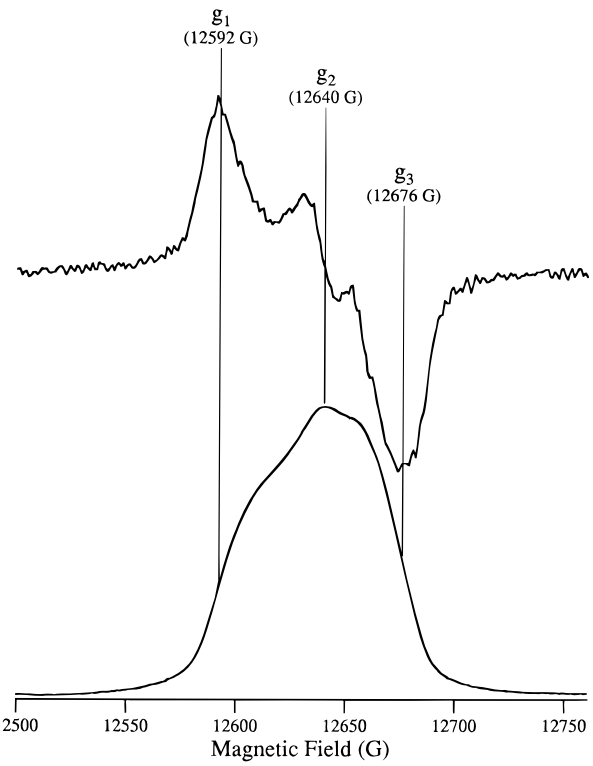

Figure 1. Q-band dispersion-mode rapid-passage EPR spectrum of **X** (*lower)*. The numerical derivative, which approximates a conventional derivative-display, absorption-mode spectrum also is shown (*upper*). *Conditions*: Microwave frequency, 35.364 GHz; modulation amplitude, 0.68G; T = 2 K.

Results

EPR Spectroscopy. Although **X** shows an isotropic, free-radical-like EPR signal in spectra taken at X band, at Q band the signal displays the pattern of a rhombic *g*-tensor[49] with g_1 ∼ 2.007, g_2 ∼ 1.999, and g_3 ∼ 1.994 (Figure 1). This degree of anisotropy is sufficient to permit the use of ENDOR to estimate full hyperfine tensors through the procedure of acquiring orientation-selective spectra at numerous fields throughout the EPR envelope.[48]

^{57}Fe ENDOR Spectroscopy. At radio frequencies above ∼ 45 MHz, Q-band ENDOR spectra of **X** exhibit an array of hyperfine-split ^{1}H doublets centered at the proton Larmor frequency, ∼53 MHz.[36] For ^{56}Fe (natural-abundance) **X**, resonances from ^{14}N histidyl ligands occur in the region $\nu \leq$ 15 MHz, but no signals are present in the range, ∼15 < ν < ∼45 MHz.[36] As shown in Figure 2, when **X** is prepared with ^{57}Fe, doublets from two ^{57}Fe ions appear, one in the range ∼30−40 MHz and denoted Fe_A, the other in ∼ 15−20 MHz and denoted Fe_B. Although the pattern for Fe_A is distorted in this spectrum because of the spectrometer conditions (this is readily accommodated, as shown below), nonetheless it can be seen that the $\nu_- = |A/2| - \nu_{Fe}$ branch of the Fe_A pattern is more intense than the $\nu_+ = |A/2| + \nu_{Fe}$ branch, whereas the relative intensities of the two branches are reversed for Fe_B. Such unequal intensities are common in cw Q-band ENDOR spectroscopy; in this instance the different sense of the intensity disparity for Fe_A and Fe_B undoubtedly reflects the fact that their hyperfine interactions have different signs (see below).

(40) However, the results of control experiments performed on **X** generated from wild-type R2 are indistinguishable from those presented here. Williams, J.-P; Burdi, D.; Stubbe, J.; Hoffman, B. M., unpublished observation.

(41) Thelander, L. *J. Biol. Chem.* **1973**, *248*, 4591−4601.
(42) Ballou, D. P.; Palmer, G. *Anal. Chem.* **1974**, *46*, 1248.
(43) Bray, R. C. *Biochem. J.* **1961**, *81*, 189.
(44) Werst, M. M.; Davoust, C. E.; Hoffman, B. M. *J. Am. Chem. Soc.* **1991**, *113*, 1533−1538.
(45) Hoffman, B. M.; DeRose, V. J.; Ong, J. L.; Davoust, C. E. *J. Magn. Reson.* **1994**, *110*, 52−57.
(46) Hoffman, B. M.; Gurbiel, R. J.; Werst, M. M.; Sivaraja, M. In *Advanced EPR. Applications in Biology and Biochemistry*; Hoff, A. J., Ed.; Elsevier: Amsterdam, 1989; pp 541−591.
(47) Hoffman, B. M. *Acc. Chem. Res.* **1991**, *24*, 164−170.
(48) Hoffman, B. M.; DeRose, V. J.; Doan, P. E.; Gurbiel, R. J.; Houseman, A. L. P.; Telser, J. In *EMR of Paramagnetic Molecules*; Biological Magnetic Resonance 13; Berliner, L. J., Reuben, J., Eds.; Plenum Press: New York, 1993; pp 151−218.
(49) Wertz, J. E.; Bolton, J. R. *Electron spin resonance: elementary theory and practical applications*, 2nd ed.; Chapman and Hall: New York, 1986.

Table 1. ^{57}Fe Hyperfine Parameters for Carboxylate-Bridged Diiron Intermediates[a]

intermediate[b]	Fe site	A_1 (MHz)	A_2 (MHz)	A_3 (MHz)	ΔE_Q (mm/s)	δ (mm/s)	η	ref
X	A	−74.2 (2)	−72.2 (2)	−73.2 (2)	−0.9 (1)	0.56 (3)	0.5 (2)	this work
	B	+27.5 (2)	+36.8 (2)	+36.8 (2)	−0.6 (1)	0.26 (4)	2.7 (3)	
$[Fe_2(O)_2(6MeTPA)_2]^{3+}$	A	−64.5 (20)	−64.5 (20)	−64.5 (20)	1.6 (2)	0.48 (3)	1.0 (3)	59
	B	+20 (3)	+36.5 (15)	+36.5 (15)	0.5 (1)	0.08 (3)	1.0 (3)	
Mc **Q**	A				0.68 (3)	0.21 (2)		23, 50
	B				0.55 (3)	0.14 (2)		
Mt **Q**	A & B				0.53	0.17 (2)		52
Mc $\mathbf{H}_{peroxo}$	A & B				1.51 (3)	0.66 (2)		23, 50

[a] Magnetic hyperfine coupling constants (A_i) for **X** from ENDOR, other parameters from Mössbauer spectroscopy. Uncertainties in last digit, in parentheses. [b] **X**: intermediate **X** from RNR; 6MeTPA: *N*-(6-methyl-2-pyridylmethyl)-*N*,*N*-bis(2-pyridylmethyl)amine; **Q**: intermediate **Q** of methane monooxygenase hydroxylase; $\mathbf{H}_{peroxo}$: peroxo intermediate of methane monooxygenase hydroxylase; *Mc*: *Methylococcus capsulatus* (Bath); *Mt*: *Methylosinus trichosporium* OB3B.

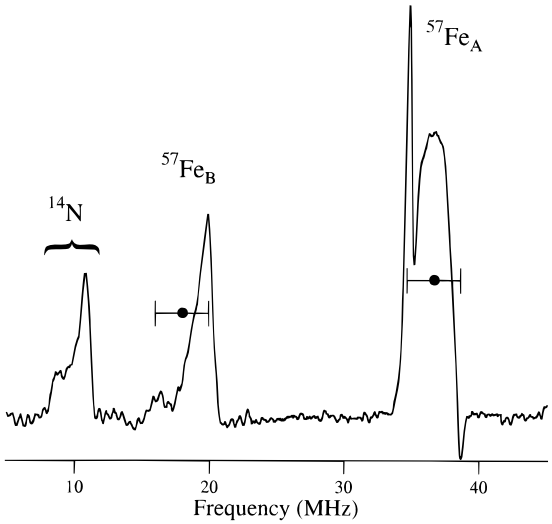

Figure 2. Representative 35-GHz CW-ENDOR spectrum taken at the high-field, g_3 edge (12 640 G) of the EPR envelope of ^{57}Fe-enriched Intermediate **X**. The transitions are assigned to ^{14}N (ν < 15 MHz), $^{57}Fe_B$ (15 < ν < 22 MHz), and $^{57}Fe_A$ (32 < ν < 40 MHz); the spectrum of an unenriched sample is featureless above ∼15 MHz. Experimental conditions optimize the $^{57}Fe_B$ ENDOR transition. See Figure 3 for experimental conditions specific to $^{57}Fe_A$ or $^{57}Fe_B$.

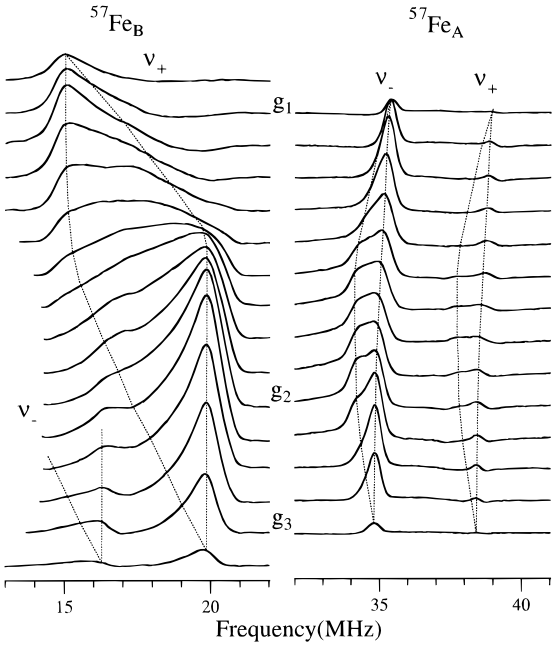

Figure 3. Optimized 35-GHz CW-ENDOR data for $^{57}Fe_A$ (right) and $^{57}Fe_B$ (left) collected at equal *g*-increments (0.0016; ∼10G) across the EPR envelope of ^{57}Fe-enriched intermediate **X**. The EPR spectrum of the ^{57}Fe-enriched sample exhibits considerable hyperfine broadening, hence the *g*-value labels indicate turning points in the EPR spectrum; these occur at g_1, 2.008; g_2, 2.000; g_3, 1.990. *Conditions*: microwave frequency, 35.3 GHz (Fe_A), 35.2 GHz (Fe_B); modulation frequency, 100 kHz; modulation amplitude, 3.7 G_{pp}; RF sweep, 0.5 MHz/s (Fe_A), 1 MHz/s (Fe_B).

^{57}Fe ENDOR spectra for both Fe_A and Fe_B have been taken under optimized conditions at numerous field/g values across the EPR envelope, as illustrated in Figure 3. Focussing on the data for ^{57} Fe_A, the spectrum taken near g_3 is a doublet centered at $A(Fe_A)/2 = -36.6$ MHz; the sign of the hyperfine coupling has been determined in our earlier Mössbauer study.[31] The center of the pattern is nearly invariant as the field of observation is moved across the EPR envelope, which means the Fe_A hyperfine coupling is virtually isotropic. The broadening of the ν_- pattern in the vicinity of g_2 shows the presence of a minimal (∼3%) anisotropy; an analysis like that described below for Fe_B indicates that the Fe_A hyperfine tensor is roughly coaxial with **g** and has principal value of **A** (Fe_A) = [−74.2, −72.2, −73.2] MHz, with isotropic component $A(Fe_A) = -73.2$ (Table 1).

The g_3 signal of $^{57}Fe_B$ in Figure 3 has a sharp peak at $\nu_+ =$ 20.2 MHz and is centered at $A(Fe_B)/2 = +18.4$ MHz (after corrections for sweep artifacts), where the sign again was determined earlier. As the field is decreased across the EPR envelope to g_2, the frequency of the intensity maximum of the ν_+ feature remains essentially invariant while the pattern gradually extends towards lower frequency, reaching ∼16 MHz by g_2. As the field is further lowered toward g_1 the intensity at ∼16 MHz rapidly builds, while the high-frequency edge of the pattern decreases rapidly in intensity and shifts to lower frequency. By g_1, $\nu_+ = 15.5$ MHz and $A(Fe_B) = +27.5$ MHz (corrected). Taking into account the fact that in the EPR signal of **X** the ^{57}Fe hyperfine broadening is *not* vanishingly small compared to the width of the EPR envelope even at Q band (data not shown), the variation of the ENDOR signal as a function of the observing field unambiguously reflects the classic pattern of ν_+ for a nucleus with a strongly anisotropic hyperfine tensor that is axially symmetric with the unique axis along g_1;[46−48] the tensor components are $A_{||} = A_1 = +27.5$ MHz, $A_\perp = A_2 = A_3 = +36.8$ (Table 1).

Mössbauer Spectroscopy. Figure 4 shows the Mössbauer spectra of ^{57}Fe-enriched **X**. The data were recorded at 4.2K with a magnetic field of 60 mT applied parallel (Figure 4A) and perpendicular (Figure 4B) to the γ-radiation. In addition to the spectrum of **X**, the data also show the absorption from the reduced diferrous center, in the form of a quadruple doublet which partially overlaps with the spectral component originating from Fe_B of **X**. This partial overlap was the main reason that the parameters of Fe_B could not be determined with certainty in the previous study.[31] Taking advantage of the ^{57}Fe hyperfine tensors determined by ENDOR, the Mössbauer data of **X** were reanalyzed. The solid lines plotted over the experimental data in Figure 4 are the theoretical simulations of **X** using the

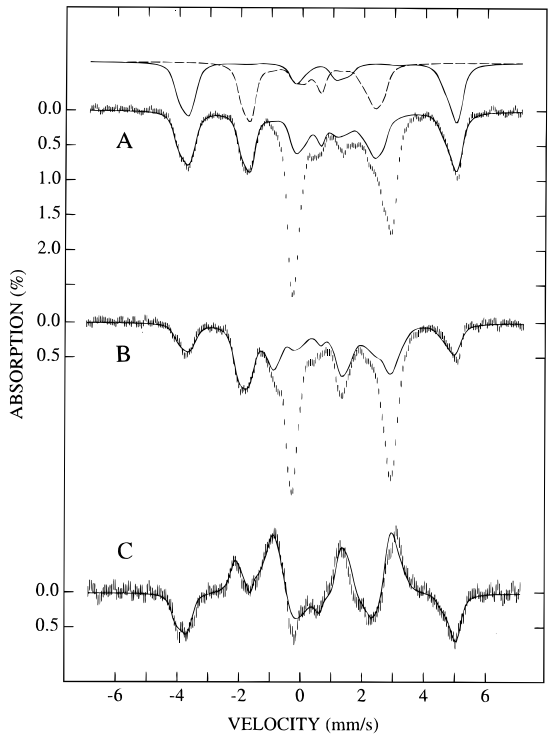

Figure 4. Mössbauer spectra at 4.2K of a rapid freeze-quenched sample from the reaction of apo R2-Y122F with 3 equiv of Fe^{2+} in the presence of O_2 and ascorbate. The reaction was quenched at 310 ms, at which time the amount of **X** is maximized. The data were recorded with a magnetic field of 60 mT applied (**A**) parallel and (**B**) perpendicular to the γ-radiation. The difference spectrum, **A** − **B**, is shown in **C**. The solid lines plotted over the experimental data are simulations of ***X*** using the parameters list in Table 1 but simplified to an isotropic A value of −73 MHz for Fe_A and axial **A** tensor ($A_{\|} = A_1 = +27.4$ MHz and $A_{\perp} = A_2 = A_3 = +37$ MHz) for Fe_B. Simulations of the parallel field spectra for individual iron sites are shown at the top of the figure: Fe_A (—) and Fe_B (– –).

parameters listed in Table 1 and the Figure legend. In comparison with the previous analysis, better agreement between experiment and theory is obtained. The major difference from the previous study is the small isomer shift of 0.26 mm/s for Fe_B, a value significantly smaller than the earlier one of 0.36 mm/s.[31] In order to demonstrate the goodness of fit of the current analysis, the difference spectrum of spectra shown in Figure 4A,B is displayed in Figure 4C and compared with the theoretical simulation (solid line). Because the diferrous center is an integer-spin system which exhibits a spectrum independent of the direction of a small applied field, its contribution to the Mössbauer data is canceled in such a difference spectrum. In other words, spectrum 4C shows only the field-direction dependence of the spectrum of **X**. Clearly, the current analysis completely describes the field-direction dependence of the Mössbauer spectrum of **X**.

Discussion

In the past few years much effort has gone into learning why protein-bound diferrous clusters that appear similar, nonetheless react with O_2 to generate intermediates with diverse chemical reactivities. The diferrous form of hemerythrin[20] binds O_2 reversibly to generate a diferric peroxide bound terminally to one of the iron ions. In contrast, the diferrous form of methane monooxygenase binds O_2 to form a diamagnetic intermediate that has been described as a symmetrically bridged diferric peroxide[50] based on the observation of a symmetrical quadrupole doublet in its Mössbauer spectrum (Table 1) and the single ^{18}O-^{16}O-sensitive stretch at 905 cm^{-1} in its resonance Raman spectrum.[51] This intermediate then reacts to form **Q**, whose structure has been formulated as, among other possibilities, a di-μ-oxo-bridged di-Fe^{IV} complex.[23,52] The Mössbauer spectrum for this intermediate from *Methylosinus trichosporium* is a symmetrical quadrupole doublet ($\delta = 0.17$ mm s^{-1}, $\Delta E_Q = 0.53$ mm s^{-1})[52], while that from *Methylococcus capsulatus* (Bath) appears as two unresolved quadrupole doublets ($\delta_1 = 0.21$ mm s^{-1}, $\Delta E_{Q1} = 0.68$ mm s^{-1}; $\delta_2 = 0.14$ mm s^{-1}, $\Delta E_{Q2} = 0.55$ mm s^{-1}).[23] The 0.49 mm s^{-1}decrease in isomer shift upon the conversion of the diferric peroxide to **Q** (Table 1) is diagnostic of a one-electron oxidation of each of the iron ions. **Q** is kinetically competent to catalyze the two-electron hydroxylation of methane to methanol. In contrast, the diferrous form of the R2 subunit of RNR reacts with O_2 and an external reductant to generate the intermediate **X** studied here, whose function is the one-electron oxidation of Y122 to the •Y122. Recent Mössbauer analysis of RNR has detected a potential new intermediate[53] that has properties similar to the diferric peroxide of MMO ($\delta \cong 0.66$ mm s^{-1} and $\Delta E_Q \cong 1.5$ mm s^{-1}) and that appears prior to the formation of **X**. The structures of both the diferrous and diferric forms of MMO hydroxylase from *M. capsulatus* (Bath)[24,54] and R2[10,55] have been solved to high resolution, and they reveal metal-ligand coordination environments that are remarkably similar to one another. An important goal of our current research is to understand the distinctive structural factors that mediate conversion of the diferric peroxide to **Q** in MMO, in contrast to the conversion of a putative diferric peroxide to **X** during RNR cofactor assembly. A key objective toward understanding the different reactivities of **X** and **Q**, their ability to mediate a one versus a two-electron oxidation, is to elucidate in detail their structures.

The extension of RFQ technology to Q-band ENDOR has provided us with an opportunity to evaluate and refine the hyperfine interactions associated with **X** and thereby afford a more complete description of its electronic structure. The opposite signs of the hyperfine couplings for Fe_A and Fe_B listed in Table 1 indicate that the Fe ions are part of an exchange-coupled center in which the two spins are aligned parallel and antiparallel to the net $S = 1/2$ system spin. The initial determination of isomer shifts of 0.55 and 0.36 mm s^{-1} for **X** and the assumption of isotropic **A** tensors for Fe_A and Fe_B suggested that they both be formulated as high-spin Fe^{III} (d^5, $S = 5/2$). This assignment requires the presence of an additional $S = 1/2$ radical spin-coupled to the diiron center in order to achieve the $S = 1/2$ ground state of **X**; this radical was proposed to be a ligand radical, oxygen being one of several options considered.[31] The new results obtained from RFQ ENDOR experiments compel us to reformulate the original spin-coupling model describing **X**.

The essentially isotropic hyperfine coupling of Fe_A (Table 1) is indeed diagnostic of the half-filled, d^5 shell of a high-spin (d^5; $S = 5/2$) ferric ion in the N/O coordination environment of RNR. For comparison, ^{57}Fe ENDOR shows that the Fe^{III} ion of the carboxylate-bridged mixed-valence (Fe^{III}:Fe^{II}) center of

(50) Liu, K. E.; Wang, D.; Huynh, B. H.; Edmondson, D. E.; Salifoglou, A.; Lippard, S. J. *J. Am. Chem. Soc.* **1994**, *116*, 7465−7466.
(51) Liu, K. E.; Valentine, A. M.; Qiu, D.; Edmondson, D. E.; Appleman, E. H.; Spiro, T. G.; Lippard, S. J. *J. Am. Chem. Soc.* **1995**, *117*, 4997−4998.
(52) Lee, S.-K.; Fox, B. G.; Froland, W. A.; Lipscomb, J. D.; Münck, E. *J. Am. Chem. Soc.* **1993**, *115*, 6450−6451.
(53) Tong, W. H.; Edmondson, D. E.; Huynh, B. H.; Stubbe, J. *J. Am. Chem. Soc.* **1996**, *118*, 2107−2108.
(54) Rosenzweig, A. C.; Frederick, C. A.; Lippard, S. J.; Nordlund, P. *Nature* **1993**, *115*, 939−947.
(55) Nordlund, P.; Eklund, H. *Current Opinion Struct. Biol.* **1995**, *5*, 758−766.

the hydroxylase component of MMO from *M. capsulatus* (Bath) has a hyperfine tensor of $\mathbf{A} = [-65, -70, -72]$ MHz when DMSO is present.[56] Likewise, the Fe_A isomer shift ($\delta = 0.55$) is highly characteristic of a ferric ion in an N/O environment. However, the electronic properties of Fe_B differ significantly from those of ferric Fe_A. The present ENDOR study shows a large hyperfine-tensor anisotropy for Fe_B (Table 1), which is atypical of a high-spin ferric with N/O coordination.[57] The determination of an isomer shift of only 0.26 mm s^{-1} for this ion upon re-evaluation of the Mössbauer data is indicative of a greater extent of oxidation. Given that **X** is oxidized by 1 equiv above the diferric state of resting R2, that it is an exchange-coupled system involving two antiferromagnetically coupled Fe ions, and that only one of these can be described as being in the high-spin ferric state (d^5, $S = 5/2$), then the appropriate description of the spin coupling in **X** is one in which Fe_A is high-spin Fe^{III}, Fe_B is high-spin Fe^{IV} (d^4, $S = 2$), and antiferromagnetic exchange between Fe_A and Fe_B produces the observed $S = 1/2$ ground state.

There are few systems that provide appropriate comparisons to **X**. The assignment of Fe_B as high-spin Fe^{IV}, rather than as an Fe^{III} involved in spin coupling to a radical, is supported by results for a recently-synthesized complex that contains a high-spin ferric ion (N/O environment) coordinated to a phenoxyl radical.[58] Strong antiferromagnetic exchange between the radical and metal ion causes the pair to behave as an $S = 2$ system, yet the metal ion retains a characteristic ferric-ion isomer shift, $\delta = 0.54$ mm s^{-1}. There are only two model compounds[59,60] and only one biological center, **Q**, that contain high-spin Fe^{IV} for comparison with X.[23,52] The di-μ-oxo diiron complex recently formulated by Que and co-workers in terms of antiferromagnetically coupled high-spin Fe^{III}/Fe^{IV} [59] is the most appropriate model system and will be compared in detail.[61] Both **X** and the model complex are similar in that each is a spin-coupled diiron system whose X-band EPR spectrum is a sharp isotropic singlet at $g = 2.00$. This requires that each Fe^{IV} has a strongly covalent environment that leads to a ligand-field splitting of its d-manifold where the sum of the rhombic and tetragonal distortions is large. Furthermore the isomer shift of the Fe^{III} site of the model complex (0.48 mm s^{-1}) compares well with Fe_A in **X** (0.56 mm s^{-1}). However, the isomer shift for the Fe^{IV} site of the model complex (0.08 mm s^{-1}) is significantly lower than that found for Fe_B of **X** (0.26 mm s^{-1}), although in part this discrepancy undoubtedly arises from the nitrogen-rich ligand environment of the model compound relative to **X**.

It is instructive to compare the ^{57}Fe hyperfine tensors of **X** and the model. For an exchange-coupled [Fe^{III}($S = 5/2$); Fe^{IV}-($S = 2$)] diiron center, the observed hyperfine tensors, **A**, are related to the intrinsic tensors of the uncoupled ions, **a**, by the relationships, $\mathbf{A}(Fe^{III}) = 7\mathbf{a}(Fe^{III})/3$; $\mathbf{A}(Fe^{IV}) = -4\mathbf{a}(Fe^{IV})/3$. The resulting intrinsic isotropic hyperfine coupling for ferric Fe_A of **X**, $a = -31.4$, is in good agreement with $a = -28-30$ MHz reported for Fe sites with octahedral N/O coordination.[62] The fact that both **X** and the model have EPR signals near $g = 2.0$ means that orbital contributions to their magnetic properties are minimal.[49,56] As a result of this, the hyperfine tensor of the Fe^{IV} for both systems arises almost exclusively from contributions made by isotropic (Fermi contact) and dipolar coupling terms. For **X**, the intrinsic isotropic part of $\mathbf{a}(Fe_B)$ ($a = -25.3$ MHz) compares very well with the value $a = -23.2$ MHz for the Fe^{IV} site in the Fe^{III}/Fe^{IV} di-μ-oxo model compound; the intrinsic anisotropic dipolar contribution to $\mathbf{a}(Fe_B)$ of **X** ($\Delta\mathbf{a} = a_{||} - a_{\perp} = 7.0$ MHz) is only 56% that of $\mathbf{a}(Fe^{IV})$ of the model, where $\Delta\mathbf{a} = 12.4$ MHz.

The reduced dipolar anisotropy seen for Fe_B of **X**, relative to Fe^{IV} of the model of Dong et al., represents an additional delocalization of spin density onto ligands of Fe_B. The relative extent of this delocalization for the Fe^{IV} ions of the two systems can be estimated by comparing their $\Delta\mathbf{a}$. For heuristic purposes we may imagine that unpaired spin is delocalized onto oxygen through the antibonding Fe_B-ligand orbital that involves a single "cloverleaf" d-orbital of iron,[63] in which case, $\Delta\mathbf{a} = (3/2)[4P/(7(2S))]c^2$,where $S = 2$ and $P = g\beta_n g_n \beta_n \langle r^{-3}\rangle/h$ is the dipolar hyperfine interaction constant for a d-electron. In the simplest picture, c is the coefficient of the d-cloverleaf in this metal-ligand orbital and c^2 is the spin density on Fe_B associated with this orbital. If we adopt the value $P = 85$ MHz,[62] the respective $\Delta\mathbf{a}$ for Fe^{IV} of the model compound and for Fe_B of **X** suggest that approximately 35% and 62% of an electron is delocalized onto Fe^{IV} from oxygen in the two centers. When considered together with the intermediate value of the isomer shift for Fe_B, this analysis suggests that, although the d^4 electron configuration and Fe^{IV} valency for this ion are the appropriate formal description for discussing spin coupling in **X**, the actual situation involves an intermediate charge distribution and substantial spin delocalization onto the ligand(s) of Fe_B. Additional evidence for spin delocalization onto exogenous oxygenic ligand(s) in **X** is found in our recent ^{17}O ENDOR study,[36] reminiscent of the delocalization found by ^{17}O ENDOR study of the intermediate-spin ($S = 1$) oxo-ferryl, $[Fe^{IV}O]^{2+}$, moiety of horseradish peroxidase compound I.[64] A more complete description of the delocalization in both **X** and the model of Dong et al. likewise should be available from detailed analysis of ^{17}O ENDOR measurements.

Only preliminary comparisons are possible between **X** and the first characterized non-heme Fe^{IV} center in a biological system, intermediate **Q** in the methane monooxygenase system.[23,52] This compound, formulated as a di-Fe^{IV} species, has Mössbauer parameters (ΔE_Q and δ) similar to those of Fe_B in **X**, indicating similar charge distribution for the Fe^{IV} ions in

(56) DeRose, V. J.; Liu, K. E.; Lippard, S. J.; Hoffman, B. M. *J. Am. Chem. Soc.* **1996**, *118*, 121−134.

(57) We note, however, that significant anisotropy in **A** and reduced isomer shifts have been reported for the high-spin ferric site of the more-covalent, all-sulfur coordinated $[2Fe,2S]^{1-}$ center in ferredoxins (Münck, E.; Debrunner, P. G.; Tsibris, J. C. M.; Gunsalus, I. C. *Biochemistry* **1972**, *11*, 855−863. Barata, B. A. S.; Liang, J.; Moura, I.; LeGall, J.; Moura, J. J. G.; Huynh, B. H. *Eur. J. Biochem.* **1992**, *204*, 773−778.).

(58) (a) The complex is the monocation created by one-electron oxidation of the neutral complex between Fe^{III} and triazacyclononane macrocycle to which is appended three phenolato ligands. (Weighardt, K., personal communication). (b) For related, earlier work, see: Hockertz, J.; Steenken, S.; Wieghardt, K.; Hildebrandt, P. *J. Am. Chem. Soc.* **1993**, *115*, 11222−11230.

(59) Dong, Y.; Que, L., Jr.; Kauffmann, K.; Münck, E. *J. Am. Chem. Soc.* **1995**, *117*, 11377−11378.

(60) Kostka, K. L.; Fox, B. G.; Hendrich, M. P.; Collins, T. J.; Rickard, C. E.; Wright, L. J.; Münck, E. *J. Am. Chem. Soc.* **1993**, *115*, 6746−6757.

(61) The first isolated high spin Fe^{IV} model complex, the mononuclear tetraamido-N-liganded Fe^{IV} chloride of Collins and co-workers ($\delta_{Fe^{IV}} = -0.04$ mm s^{-1}) (Kostka, K. L.; Fox, B. G.; Hendrich, M. P.; Collins, T. J.; Rickard, C. E.; Wright, L. J.; Münck, E. *J. Am. Chem. Soc.* **1993**, *115*, 6746−6757.), was a key advance but is not viewed as appropriate for comparison with X in part because its intrinsic isotropic hyperfine coupling (−15 MHz) is considerably smaller than for Fe_B of **X**. In addition, although the anisotropic contribution of the Collins mononuclear Fe^{IV} is of comparable magnitude to those of the Fe^{IV} in the two dinuclear clusters, unlike **X** and the compound of Dong *et al.*, the mononuclear molecule has an intrinsic $g \sim 1.8$. This deviation from $g = 2.00$ indicates a significant orbital contribution to its magnetic properties that is absent in the dinuclear centers.

(62) Sage, J. T.; Xia, Y.-M.; Debrunner, P. G.; Keough, D. T.; de Jersey, J.; Zerner, B. *J. Am. Chem. Soc.* **1989**, *111*, 7239−7247.

(63) Recall that the net direction of charge transfer through the combined effects of the bonding *and* antibonding orbitals is from O to Fe.

(64) Roberts, J. E.; Hoffman, B. M.; Rutter, R.; Hager, L. P. *J. Am. Chem. Soc.* **1981**, *103*, 7654−7656.

the two intermediates. The magnetic hyperfine interaction of the Fe^{IV} and ^{17}O ligands of **X** cannot be compared with the equivalent parameters for **Q**, however, as the latter is diamagnetic.[52]

The extension of RFQ technology to Q-band ENDOR spectroscopy has afforded a more detailed description of the ^{57}Fe hyperfine tensors associated with **X**, which has led to the reformulation of **X** as a spin-coupled Fe^{III}/Fe^{IV} center. Continuing spectroscopic studies of this intriguing intermediate will lead to a structural model for **X** and will help to provide a clearer picture of the structural and electronic factors which govern its reactivity and distinguish it from **Q** in methane monooxygenase.

Acknowledgment. This work was supported by the NIH (Grants HL 13531(B.M.H.), GM 29595 (J.S.), GM 47295 (B.H.H.), and GM 29433 (D.E.E.) and by the American Cancer Society (Postdoctoral Fellowship to D.B.).

JA960399K